IOP Conf. Series: Journal of Physics: Conf. Series **833** (2017) 012020 doi:10.1088/1742-6596/833/1/012020

Efficient emitting molecules in organic light-emitting diodes on the basis of the control of vibronic couplings

Tohru Sato[a,b]

[a]Department of Molecular Engineering, Graduate School of Engineering, Kyoto University, Nishikyo-ku, Kyoto 615-8510, Japan
[b]Unit of Elements Strategy Initiative for Catalysts & Batteries, Kyoto University, Nishikyo-ku, Kyoto 615-8510, Japan

E-mail: tsato@moleng.kyoto-u.ac.jp

Abstract. A high external quantum efficiency observed in organic light-emitting diodes using PTZ-BZP (PTZ: 10-hexyl-phenothiazin, and BZP: 4-phenyl-2,1,3-benzothiadiazole) as an emitting molecule is studied based on the vibronic coupling density analyses employing the time-dependent density functional theory. The high efficiency can be attributed to a high efficiency of exciton generation which originates from reverse intersystem crossings from the higher T_3 and T_2 states than T_1 to the emitting S_1 state. The nonradiative transitions from T_3 and T_2 to the lower triplet states are suppressed because of small offdiagonal vibronic coupling constants. The small vibronic couplings originate from the multi-configurationality of these triplet states. A molecular design principle for efficient emitting molecules is discussed from the view of the control of vibronic couplings.

1. Introduction

Vibronic couplings play important roles in light emission from a molecule. Off-diagonal vibronic couplings give rise to nonradiative transitions, and diagonal vibronic couplings are related to the geometrical deviation of the minimum of the ground and excited state[1]. A large vibrational relaxation results in small Franck-Condon factors which give rise to a small rate constant of the radiative transition. Therefore, small diagonal and off-diagonal vibronic couplings are crucial in designing of an efficient emitting molecule.

We have proposed concepts of vibronic coupling densities (VCD) to analyze and control diagonal and off-diagonal vibronic couplings[2, 3]. On the basis of vibronic coupling density analysis, we designed efficient emitting molecules by the suppression of vibronic couplings in anthracene[4] and triphenylamine[5], and we experimentally observed the increases of quantum yields of the designed molecules[6, 7]. It should be noted that triphenylamine is known as a non-emitting molecule. We can make a non-emitting molecule fluorescent by a molecular design on the basis of a vibronic coupling density analysis.

Thermally-activated delayed fluorescence (TADF) has attracted much attention as a highly-efficient emitting mechanism for organic light-emitting diodes (OLED) [8, 9, 10, 11]. Thermally excited T_1 excitons are converted to S_1 excitons via reverse intersystem crossing. While a fluorescent OLED and a phosphorescent OLED utilize 25% singlet and 75% triplet excitons

at best, respectively, in TADF OLED, both T_1 and S_1 excitons which are generated by current excitations are utilized for light emission. The external quantum efficiency (EQE) of a fluorescent, phosphorescent, and TADF OLED is 0.05 of photoluminescence quantum yield (PLQY), 0.15 of PLQY, and 0.20 of PLQY, respectively.

We have proposed a fluorescence via higher triplets mechanism to increase the efficiency of exciton generation[12, 13, 14]. Fluorescence via reverse intersystem crossing from T_n states higher than T_1 to S_m is possible by suppressing non-radiative transitions from T_n based on the concept of vibronic coupling density as long as the energy level of T_n is close to S_m.

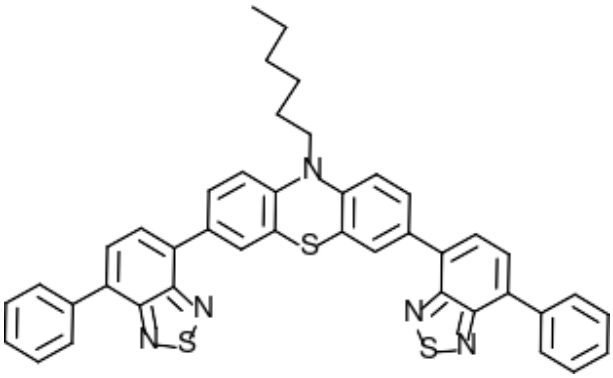

Figure 1. Molecular structure of PTZ-BZP. PTZ-BZP consists of the central 10-hexyl-phenothiazin (PTZ) moiety and the two 4-phenyl-2,1,3-benzothiadiazole (BZP) moieties.

PTZ-BZP (see figure 1) consists of the central 10-hexyl-phenothiazin (PTZ) moiety and the two 4-phenyl-2,1,3-benzothiadiazole (BZP) moieties. Yao *et al.* have reported that they observed the electroluminescence (EL) of a device using PTZ-BZP as an emitting molecule with EQE=1.54 %[15]. Since the observed PLQY was 16%, we cannot explain the observed EQE based on the fluorescent EL mechanism. In other word, triplet excitons as well as singlet ones should be utilized in this device. In this study, we analyze the EL mechanism on the basis of VCD to elucidate the high efficiency of exciton generation in the OLED of PTZ-BZP employing the time-dependent density functional theory (TD-DFT). We also propose a molecular design principle for the fluorescence via higher triplets mechanism.

2. Vibronic coupling constants and vibronic coupling density

The definitions of vibronic coupling constants and vibronic coupling densities are briefly summarized here. See details in the literature[2, 3]. Vibronic coupling operator is written as

$$\hat{V}Q_\alpha = \left(\frac{\partial \hat{H}}{\partial Q_\alpha}\right)_{\boldsymbol{R}_0} Q_\alpha, \tag{1}$$

where $\hat{H}$ is a molecular Hamiltonian, Q_α is the normal coordinate of mode α, and $\boldsymbol{R}_0$ is a reference molecular geometry.

Diagonal vibronic coupling constant (VCC) of state n is defined by

$$V_n^\alpha := \left\langle \Psi_n(\boldsymbol{R}_0, \boldsymbol{r}) \left| \hat{V}_\alpha \right| \Psi_n(\boldsymbol{R}_0, \boldsymbol{r}) \right\rangle + \left(\frac{\partial U_{nn}}{\partial Q_\alpha}\right)_{\boldsymbol{R}_0}, \tag{2}$$

where $\Psi_n(\boldsymbol{R}_0, \boldsymbol{r})$ is the electronic wavefunction of state n, and U_{nn} is the nuclear-nuclear repulsion. $\boldsymbol{r}$ denotes the coordinates of electrons. A diagonal VCC is the driving force of a

vibrational relaxation. The reorganization energy can be expressed in terms of diagonal VCCs,

$$E^n_{\rm reorg} = \sum_\alpha \frac{(V^n_\alpha)^2}{2\omega^2_\alpha}. \tag{3}$$

Offdiagonal VCC between state m and n is defined by

$$V^\alpha_{mn} := \left\langle \Psi_m(\boldsymbol{R}_0, \boldsymbol{r}) \left| \hat{V}_\alpha \right| \Psi_n(\boldsymbol{R}_0, \boldsymbol{r}) \right\rangle \tag{4}$$

A offdiagonal VCC is a driving force of a nonradiative transition. Small offdiagonal VCCs result in the suppression of a nonradiative transition.

Offdiagonal vibronic coupling density (VCD) is defined by

$$\eta^\alpha_{mn}(\boldsymbol{r}_1) := \rho_{mn}(\boldsymbol{r}_1) v^\alpha(\boldsymbol{r}_1). \tag{5}$$

VCD describes a local picture of a vibronic coupling (see Appendix). Potential derivative $v^\alpha(\boldsymbol{r}_1)$ is defined in Appendix, and overlap density $\rho_{mn}(\boldsymbol{r}_1)$ is defined by

$$\rho_{mn}(\boldsymbol{r}_1) := N \int \cdots \int d\sigma_1 d\boldsymbol{x}_2 \cdots d\boldsymbol{x}_N \Psi^*_m(\boldsymbol{R}_0, \boldsymbol{x}_1, \cdots, \boldsymbol{x}_N) \Psi_n(\boldsymbol{R}_0, \boldsymbol{x}_1, \cdots, \boldsymbol{x}_N), \tag{6}$$

where $\boldsymbol{x}_i = (\boldsymbol{r}_i, \sigma_i)$ with the space coordinates $\boldsymbol{r}_i$ and spin coordinate σ_i) of electron i. Offdiagonal VCC V^α_{mn} is the integral of offdiagonal VCD $\eta^\alpha_{mn}(\boldsymbol{r}_1)$:

$$V^\alpha_{mn} = \int \eta^\alpha_{mn}(\boldsymbol{r}_1) d\boldsymbol{r}_1. \tag{7}$$

3. Method of calculation

The ground state was optimized employing M06-2X/6-31G(d,p). The semi-empirical functional M06-2X[16] has been employed in theoretical studies on TADF molecules[9]. The optimized structure of S_0 was confirmed by performing vibrational analysis. The excited states, S_1, T_1, T_2, and T_3 were optimized by using time-dependent density functional theory (TD-DFT) at the M06-2X/6-31G(d,p) level of theory. In our preliminary investigation at the B3LYP/6-31G(d,p) level of theory[13], the calculated absorption wavelength is too long compared with the experimental value[15].

The offdiagonal vibronic coupling constants and vibronic coupling densities were calculated from the excited electronic wavefunction for the optimized geometries. These electronic and vibrational structures were obtained by Gaussian09[17]. The VCC calculations and VCD analyses were performed by using our in-house codes. The vibrational vectors employed for the VC calculations and analyses were obtained from the vibrational analysis for the S_0 states at the optimized geometries of the excited states, since only a numerical frequency analysis is available for an excited state in Gaussian09. A numerical frequency analysis is computationally very demanding.

4. Results and discussion

4.1. Franck-Condon S_1 state

Table 1 summarizes the Franck-Condon excited sates S_n@S_0 and T_n@S_0, where @S_n means that the excited states are calculated for the S_0 optimized geometry. The calculated excitation energy of S_1 reproduces the experimental absorption wavelength well.

The calculated diagonal VCCs are shown in figure 2 for the vibrational modes. A large reorganization energy, or vibrational relaxation of S_1 suppresses the rate constant of a fluorescent process[1]. The total reorganization energy was estimated to be 372 meV by using Eq.(3), which is not so large as an emitting molecule[1].

Table 1. Franck-Condon excited states calculated at the M06-2X/6-31G(d,p) level of theory.

State	Excitation energy		f	Major configurations (CI coefficient)
	eV	nm		
T_1 (^3A)	2.3225	533.85	0.0000	NHO → NLU (0.43658)
				HO → LU (0.35711)
T_2 (^3A)	2.3308	531.94	0.0000	NHO → LU (0.41920)
				HO → NLU (0.33955)
S_1 (^1A)	3.2051	386.83	0.7867	HO → LU (0.59349)
T_3 (^3A)	3.2794	378.07	0.0000	HO → LU (0.36497)
				HO → LU+2 (0.32673)
S_2 (^1A)	3.3470	370.43	0.1971	NHO → LU (0.30039)
				HO → NLU (0.58363)
Exp[15]	2.77	447		

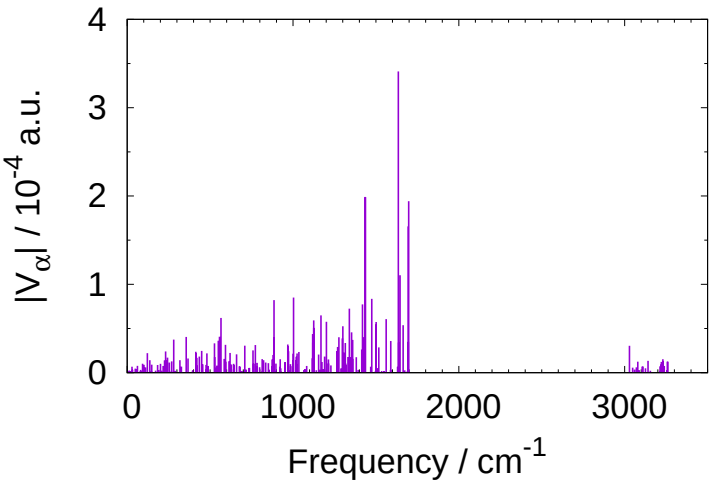

Figure 2. Diagonal vibronic coupling constants for the Franck-Condon S_1 state at the M06-2X/6-31G(d,p) level of theory.

4.2. S_1 adiabatic state

The excited states for the optimized structure of the S_1 state are tabulated in table 2. The energy levels of T_2 and T_3 are close to that of S_1. This suggests that the reverse intersystem crossing from T_2 or T_3 to S_1 could be possible if the energy levels of $T_2@T_2$ and $S_1@T_2$, or those of $T_1@T_1$ and $S_1@T_1$ are close each other with the offdiagonal VCCs between the higher triplet states and the lower ones small.

Offdiagonal vibronic couplings between S_1 and S_0 should be small as a fluorescent molecule. The offdiagonal VCCs between the $S_1@S_1$ and $S_0@S_1$ are shown in figure 3. They are less than 1×10^{-3} a.u. which is typical in a fluorescent molecule. The strong coupling modes are 7.29×10^{-4} a.u. of mode 111 (960 cm^{-1}) and 7.14×10^{-4} a.u. of mode 45 (403 cm^{-1}). We performed the VCD analyses for these modes.

Figure 4 shows the VCD analyses of the strong coupling modes, mode 111 and mode 45, for the S_1 adiabatic state. The overlap density between $S_1@S_1$ and $S_0@S_1$ is localized on the one

Table 2. S_1 adiabatic excited states calculated at the M06-2X/6-31G(d,p) level of theory.

State	Excitation energy		f	Major configurations (CI coefficient)
	eV	nm		
T_1 (^3A)	1.5619	793.81	0.0000	NHO → LU (0.42818)
				HO → LU (0.51651)
T_2 (^3A)	2.2316	555.58	0.0000	HO-2 → NLU (0.40509)
				NHO → NLU (-0.30471)
				HO → NLU (0.38302)
S_1 (^1A)	2.4851	498.92	0.6998	HO → LU (0.66212)
T_3 (^3A)	2.6813	462.40	0.0000	NHO → LU (0.34910)
				HO → LU (-0.34410)
S_2 (^1A)	3.0121	411.61	0.2710	HO → NLU (0.62714)
Exp[15]	2.10	590		

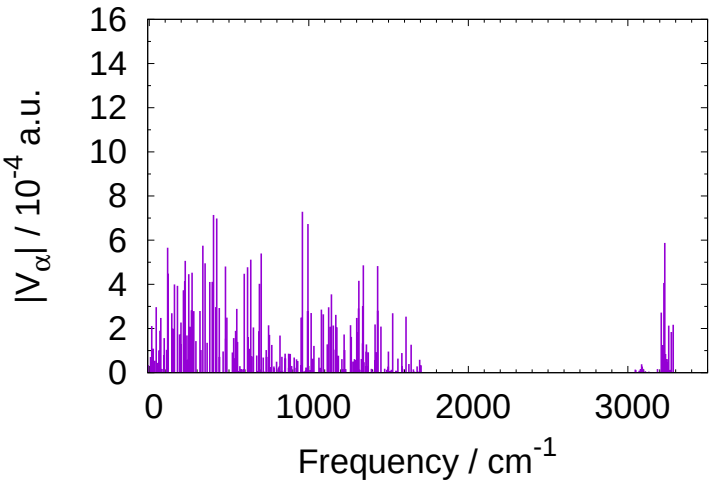

Figure 3. Offdiagonal vibronic coupling constants between S_1 and S_0 states for the adiabatic S_1 state at the M06-2X/6-31G(d,p) level of theory.

of the BZP moieties. As shown in figure 4 (c) and (e), therefore, the VCs originate from the overlap density on the BZP moiety. Accordingly, in order to enhance the PLQY, the overlap density on the BZP moiety should be reduced.

4.3. T_3 adiabatic state

The excited states for the optimized geometry of T_3 is summarized in table 3. The energy level of T_3@T_3 is close to that of S_1@T_3. The energy gap between S_1@T_3 and T_3@T_3, $\Delta E_{S_1@T_3-T_3@T_3} = 25$ meV. This small energy gap makes the thermal activation from T_3 to S_1 possible if the offdiagonal vibronic couplings are small.

Figures 5 and 7 show the offdiagonal VCCs between the T_3 and T_2 states, and the T_3 and T_1 states, respectively. The strong coupling modes between T_3 and T_2 are 3.20×10^{-4} a.u. of mode 201 (1629 cm^{-1}), and -2.87×10^{-4} a.u. of mode 177 (1420 cm^{-1}). The strong coupling modes between T_3 and T_1 are 3.62×10^{-4} a.u. of mode 78 (697 cm^{-1}), and 3.11×10^{-4} a.u.

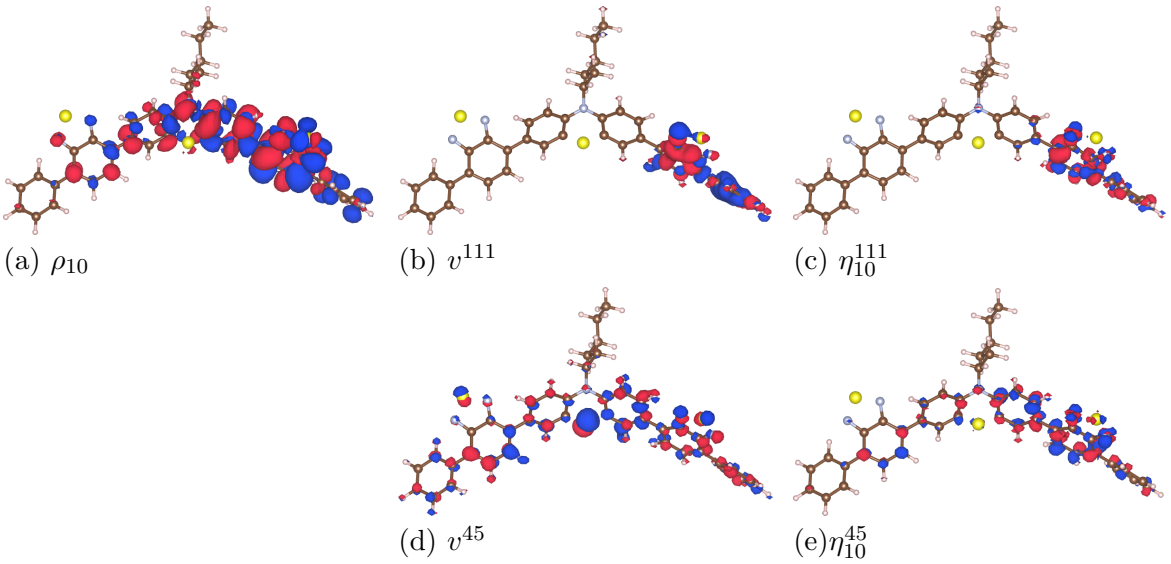

(a) ρ_{10} (b) v^{111} (c) η_{10}^{111}

(d) v^{45} (e)η_{10}^{45}

Figure 4. The VCD analyses for the S_1 adiabatic state at the M06-2X/6-31G(d,p) level of theory. Mode 111 and mode 45 indicate strong couplings. (a) Overlap density between S_1@S_0 and S_0@S_1, ρ_{10}, (b) potential derivative of mode 111, v^{111}, (c) VCD of mode 111, η_{10}^{111}, (d) potential derivative of mode 45, v^{45}, and (e) VCD of mode 45, η_{10}^{45}. The isosurface values are 5.0×10^{-4} for ρ, 0.004 for v, and 5.0×10^{-6} for η, respectively.

Table 3. T_3 adiabatic excited states calculated at the M06-2X/6-31G(d,p) level of theory.

State	Excitation energy		f	Major configurations (CI coefficient)
	eV	nm		
T_1 (^3A)	2.0115	616.39	0.0000	NHO → NLU (-0.36213)
				HO → LU (0.47322)
				HO-2 → LU (0.24834)
T_2 (^3A)	2.0799	596.09	0.0000	NHO → LU (0.41808)
				HO → NLU (-0.40890)
				HO-2 → NLU (-0.29704)
T_3 (^3A)	2.6324	471.00	0.0000	HO → LU+2 (0.39798)
				HO-2 → LU (0.28310)
				NHO → NLU (-0.25387)
				HO → LU (-0.28352)
S_1 (^1A)	2.6574	466.56	0.6657	HO → LU (0.65139)
S_2 (^1A)	2.9119	425.79	0.1057	HO → NLU (0.66925)

of mode 202 (1630 cm^{-1}). These coupling constants are rather small, which suggests that the nonradiative transitions from the T_3 state to the T_2 and T_1 states are suppressed.

4.4. T_2 adiabatic state

Table 4 summarizes the excited states for the T_2 optimized geometry. The energy gap between the T_2@T_2 and S_1@T_2 states, $\Delta E_{S_1@T_2-T_2@T_2}$ is equal to -14.9 meV. If the offdiagonal vibronic couplings between T_2 and T_1 are small, the reverse intersystem crossing from T_2 to S_1 is possible.

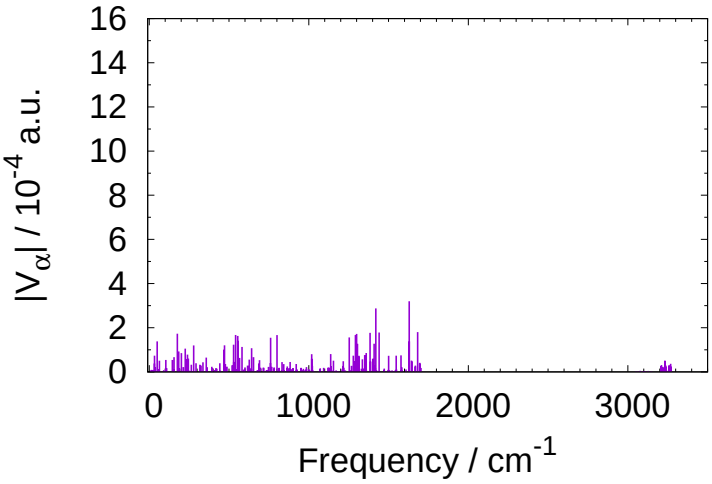

Figure 5. Offdiagonal vibronic coupling constants between T_3 and T_2 states for the adiabatic T_3 state at the M06-2X/6-31G(d,p) level of theory.

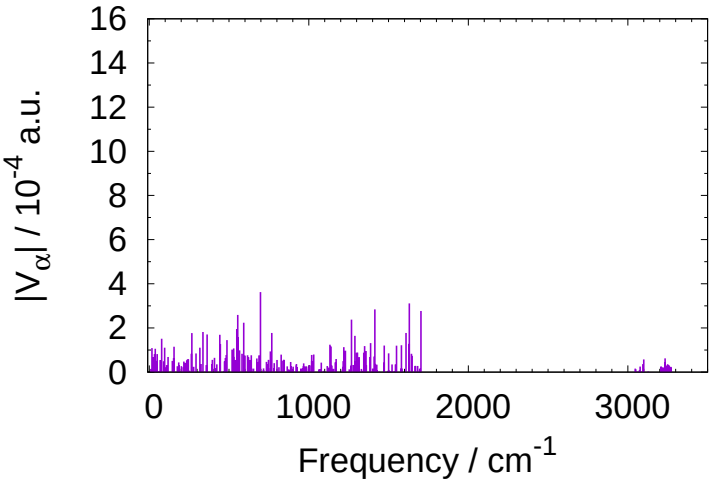

Figure 6. Offdiagonal vibronic coupling constants between T_3 and T_1 states for the adiabatic T_3 state at the M06-2X/6-31G(d,p) level of theory.

The offdiagonal VCCs between the T_2 and T_1 states are shown in figure 7. It should be noted that the order of the coupling constants is of 10^{-5} a.u. The extremely small coupling constants originate from the small overlap density discussed in the following subsection.

4.5. Reductions of the overlap densities

Figure 8 shows the overlap densities between the T_3 and T_2 states, the T_3 and T_1 states, and the T_2 and T_1 states. Note that the isosurface value (0.0005) of the overlap density between S_1 and S_0 shown in figure 4 (a) is larger than the isosurface values (0.0002) of figure 8. The overlap densities between the T_3 and T_2 states (figure 8 (a)), and the T_3 and T_1 states (figure

Table 4. T_2 adiabatic excited states calculated at the M06-2X/6-31G(d,p) level of theory.

State	Excitation energy		f	Major configurations (CI coefficient)
	eV	nm		
T_1 (^3A)	1.0565	1173.56	0.0000	NHO → LU (0.35875)
				HO → LU (0.60451)
S_1 (^1A)	2.3072	537.38	0.6700	HO → LU (0.67479)
T_2 (^3A)	2.3221	533.94	0.0000	HO-2 → NLU (0.42305)
				NHO → NLU (-0.39498)
T_3 (^3A)	2.7331	453.64	0.0000	NHO → LU (0.42675)
				HO → LU (-0.31247)
T_4 (^3A)	3.1743	390.58	0.0000	HO-10 → LU (0.50716)
				HO-9 → LU (0.34630)
S_2 (^1A)	3.1799	389.90	0.2617	NHO → LU (0.42893)
				HO → NLU (-0.40933)

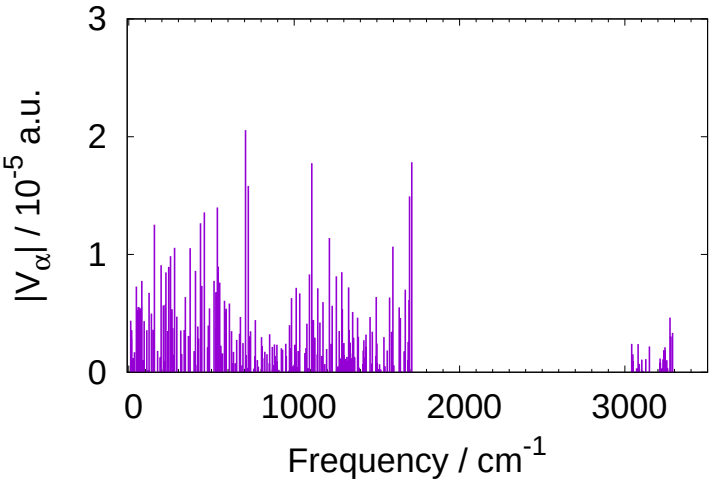

Figure 7. Offdiagonal vibronic coupling constants between T_2 and T_1 states for the adiabatic T_2 state at the M06-2X/6-31G(d,p) level of theory.

8 (b)) are reduced compared with that between the S_1 and S_0 states (figure 4 (a)). The overlap density between the T_2 and T_1 states (figure 8 (c)) are much reduced.

Compared with offdiagonal vibronic couplings between S_1 and S_0, which is a driving force of the nonradiative transition that competes with the fluorescent process, those between the higher triplet states and lower triplet ones are small in PTZ-BZP. This is one of the necessary condition for the fluorescence via higher triplets mechanism. We discuss this reductions from the view of the structures of the excited wave functions.

Overlap density between states $\Psi_1 = c_{1a}\Phi_a + c_{1b}\Phi_b$ and $\Psi_2 = c_{2c}\Phi_c + c_{2d}\Phi_d$, $\rho(\Psi_1, \Psi_2)$, can be expanded as a sum of the overlap densities between electronic configurations (Slater determinants):

$$\rho(\Psi_1, \Psi_2) = c^*_{1a}c_{2c}\rho(\Phi_a, \Phi_c) + c^*_{1a}c_{2d}\rho(\Phi_a, \Phi_d) + c^*_{1a}c_{2c}\rho(\Phi_a, \Phi_c) + c^*_{1a}c_{2d}\rho(\Phi_a, \Phi_d), \qquad (8)$$

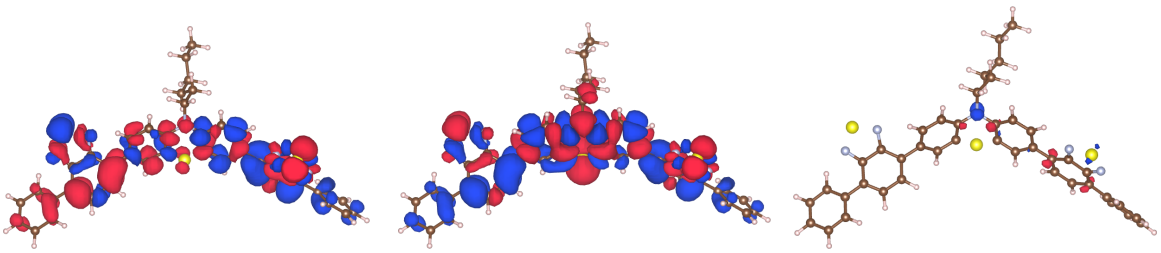

(a) ρ_{32} (b) ρ_{31} (c) ρ_{21}

Figure 8. Overlap densities between (a) $T_3@T_3$ and $T_2@T_3$, (b) $T_3@T_3$ and $T_1@T_3$, and (c) $T_2@T_2$ and $T_1@T_2$. All the isosurface values are 2×10^{-4}.

where $\Phi_i \quad (i = a, b, c, d)$ is an electronic configuration, and $c_{ki} \quad (k = 1, 2)$ is a configuration interaction (CI) coefficient.

A TD-DFT wavefunction consists of one-electron excited electronic configurations, Φ_i^r, where i denotes an occupied molecular orbital ψ_i, and r is an unoccupied molecular orbital ψ_r:

$$\Psi = \sum c_i^r \Phi_i^r. \tag{9}$$

Overlap density between the electronic configurations satisfies the following:

$$\begin{aligned}
\rho(\Phi_i^r, \Phi_i^r) &= \rho_0 - \rho_i + \rho_r, && (10)\\
\rho(\Phi_i^r, \Phi_i^s) &= \psi_r^* \psi_s, && (11)\\
\rho(\Phi_i^r, \Phi_j^r) &= \psi_i^* \psi_j, && (12)\\
\rho(\Phi_i^r, \Phi_j^s) &= 0 && (13)
\end{aligned}$$

where ρ_0 is the electron density of the ground electronic configuration Φ_0, and $\rho_a = \psi_a^* \psi_a \quad (a = i, r)$.

From table 4, the wavefunctions of triplet excited states $T_2@T_2$ and $T_1@T_2$ can be approximately expressed by

$$\begin{aligned}
\Psi_{T_2@T_2} &= a\Phi_{HO-2}^{NLU} - a\Phi_{NHO}^{NLU}, && (14)\\
\Psi_{T_1@T_2} &= b\Phi_{NHO}^{LU} + c\Phi_{HO}^{LU}, && (15)
\end{aligned}$$

respectively. Therefore, the overlap density can be written as

$$\rho(\Psi_{T_2@T_2}, \Psi_{T_1@T_2}) = -ab\psi_{NLU}^* \psi_{LU}. \tag{16}$$

It should be noted that $\rho(\Phi_{HO-2}^{NLU}, \Phi_{NHO}^{LU})$, $\rho(\Phi_{HO-2}^{NLU}, \Phi_{HO}^{LU})$, and $\rho(\Phi_{NHO}^{NLU}, \Phi_{HO}^{LU})$ are vanishing. In other words, the overlap density between $T_2@T_2$ and $T_1@T_2$ are reduced because of the multiconfigurational structure of the TD-DFT wavefunctions. Accordingly, the nonradiative transition from T_2 to T_1 is suppressed.

Similarly in the T_3 adiabatic state, from table 3, the wavefunctions of triplet excited states $T_3@T_3$, $T_2@T_3$, and $T_1@T_3$ can be approximately expressed by

$$\begin{aligned}
\Psi_{T_3@T_3} &= p\Phi_{HO}^{LU+2} + q\Phi_{HO-2}^{LU} - q\Phi_{NHO}^{NLU} - q\Phi_{HO}^{LU}, && (17)\\
\Psi_{T_2@T_3} &= p\Phi_{NHO}^{LU} - p\Phi_{HO}^{NLU} - q\Phi_{HO-2}^{NLU}, && (18)\\
\Psi_{T_1@T_3} &= -p\Phi_{NHO}^{NLU} + r\Phi_{HO}^{LU} + s\Phi_{HO-2}^{LU}, && (19)
\end{aligned}$$

where $p \approx 0.4$, $q \approx 0.3$, $r \approx 0.5$, and $s \approx 0.2$. The overlap densities are derived as follows:

$$\rho(\Psi_{T_3@T_3}, \Psi_{T_2@T_3}) = -p^2\psi^*_{LU+2}\psi_{NLU} + p(p+q)\psi^*_{HO-2}\psi_{NHO} - q^2\psi^*_{LU}\psi_{NLU}. \quad (20)$$

$$\begin{aligned}\rho(\Psi_{T_3@T_3}, \Psi_{T_1@T_3}) = {} & pr\psi^*_{LU+2}\psi_{LU} + q(r-s)\psi^*_{HO-2}\psi_{HO} \\ & +qs(\rho_0 - \rho_{HO-2} + \rho_{LU}) + qp(\rho_0 - \rho_{NHO} + \rho_{NLU}) \\ & -qr(\rho_0 - \rho_{HO} + \rho_{LU}) \end{aligned} \quad (21)$$

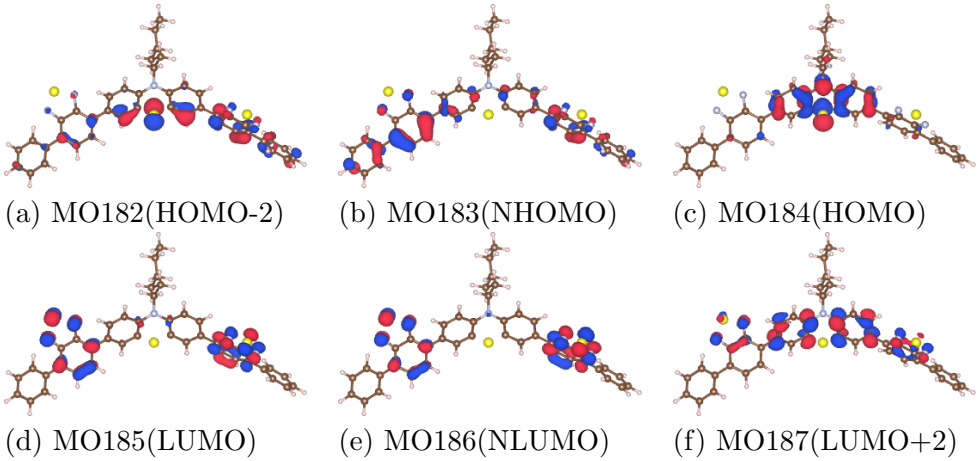

(a) MO182(HOMO-2) (b) MO183(NHOMO) (c) MO184(HOMO)

(d) MO185(LUMO) (e) MO186(NLUMO) (f) MO187(LUMO+2)

Figure 9. Frontier orbitals for the $T_3@T_3$ states at the M06-2X/6-31G(d,p) levels of theory.

As shown in figure 9, $\psi^*_{LU+2}\psi_{NLU} \approx 0$, $\psi^*_{LU+2}\psi_{LU} \approx 0$, $\psi^*_{HO-2}\psi_{NHO} \approx 0$, and $\psi^*_{HO-2}\psi_{HO} \approx 0$,

$$\rho(\Psi_{T_3@T_3}, \Psi_{T_2@T_3}) = -q^2\psi^*_{LU}\psi_{NLU}, \quad (22)$$

$$\begin{aligned}\rho(\Psi_{T_3@T_3}, \Psi_{T_1@T_3}) = {} & +qs(\rho_0 - \rho_{HO-2} + \rho_{LU}) + qp(\rho_0 - \rho_{NHO} + \rho_{NLU}) \\ & -qr(\rho_0 - \rho_{HO} + \rho_{LU}). \end{aligned} \quad (23)$$

The orbital localizations give rise to the reduction of the overlap densities.

5. Conclusion

The pseudodegenerate electronic structure can give rise to the excited state wavefunctions with the multi-configurationality. Offdiagonal VCCs between such excited state wavefunctions can be small because of the reductions of the overlap densities between them. Small VCCs make nonradiative transitions from the higher triplet states to the lower triplet states suppressed. If the energy levels of these excited state, T_2 and T_3 in PTZ-BZP, are close to the emitting state, S_1 in PTZ-BZP, the reverse intersystem crossings from the higher triplet states to the emitting state is possible (fluorescence via higher triplets mechanism). The efficiency of exciton generation in such a system can be high because both single and triplet excitons can be utilized under current excitation as is the same in TADF OLED.

For PTZ-BZP, the energy gap between S_1 and T_3 is 25 meV, and that between S_1 and T_2 is -15 meV. The offdiagonal VCCs between the T_3 and T_2 states and those between the T_3 and T_1 states are less than 3.7×10^{-4} a.u., and those between the T_2 and T_1 states are less than 2×10^{-5} a.u. Therefore, the high EQE in PTZ-BZP can be attributed to fluorescence via higher triplet states because of the suppression of the nonradiative transitions from the T_3 and

T_2 states. Since the triplet excitons can be converted to the S_1 state via reverse intersystem crossing from these higher triplet states, the efficiency of exciton generation is increased.

To increase EQE, not only the efficiency of exciton generation should be increased, but also the PLQY should be enhanced. From the offdiagonal VCD analysis for the S_1 state, the overlap density on the benzothiadiazole moieties should be reduced by some chemical modification to increase the PLQY of PTZ-BZP.

One class of the candidates of the fluorescence via higher triplets mechanism is a set of molecules of X-Y-X type. For PTZ-BZP, BZP is X, and PTZ is Y. Two same moieties of X can yield a pseudodegenerate electronic structure which can give rise to multiconfigurational excited states.

Acknowledgments
Numerical calculations were partly performed at the Supercomputer Laboratory of Kyoto University. This study was also supported by a Grant-in-Aid for Scientific Research (C) (15K05607) from the Japan Society for the Promotion of Science (JSPS).

Appendix
Vibronic coupling density operator
The field operators of an electron are defined by

$$\hat{\psi}(\boldsymbol{r}_1) := \sum_b \psi_b(\boldsymbol{r}_1)\hat{c}_b, \tag{24}$$

$$\hat{\psi}^\dagger(\boldsymbol{r}_1) := \sum_a \psi_a^*(\boldsymbol{r}_1)\hat{c}_a^\dagger, \tag{25}$$

where $\psi_b(\boldsymbol{r}_1)$ denotes a molecular orbital, and $\hat{c}_b$ and $\hat{c}_a^\dagger$ are a annihilation and creation operator, respectively.

In second-quantized form, vibronic coupling density operator[18] is written as

$$\hat{\eta}^\alpha(\boldsymbol{r}_1) := \hat{\psi}^\dagger(\boldsymbol{r}_1)v^\alpha(\boldsymbol{r}_1)\hat{\psi}(\boldsymbol{r}_1) = \sum_{a,b}\eta_\alpha^{ab}(\boldsymbol{r}_1)\hat{c}_a^\dagger\hat{c}_b, \tag{26}$$

where potential derivative $v^\alpha(\boldsymbol{r}_1)$ is defined by

$$v^\alpha(\boldsymbol{r}_1) := \left(\frac{\partial u(\boldsymbol{r}_1)}{\partial Q_\alpha}\right)_{\mathbf{R}_0}, \text{with} \quad u(\boldsymbol{r}_1) = -\sum_A \frac{Z_A e^2}{4\pi\epsilon_0\left|\boldsymbol{r}_1 - \boldsymbol{R}_A\right|}. \tag{27}$$

Orbital vibronic coupling density (OVCD) $\eta_{ab}^\alpha(\boldsymbol{r}_1)$ is defined by

$$\eta_{ab}^\alpha(\boldsymbol{r}_1) := \psi_a^*(\boldsymbol{r}_1)v^\alpha(\boldsymbol{r}_1)\psi_b(\boldsymbol{r}_1). \tag{28}$$

Offdiagonal VCC V_{mn}^α can be written by using VCD operator as

$$V_{mn}^\alpha = \langle\Psi_m\left|\hat{\eta}^\alpha\right|\Psi_n\rangle = \int \eta_{mn}^\alpha(\boldsymbol{r}_1)d\boldsymbol{r}_1. \tag{29}$$

VCD $\eta_{mn}^\alpha(\boldsymbol{r}_1)$ and OVCD $\eta_{ab}^\alpha(\boldsymbol{r}_1)$ describe a local picture of a vibronic coupling of mode α.

References

[1] Uejima M, Sato T, Yokoyama D, Tanaka K and Park J -W 2014 *Phys. Chem. Chem. Phys.* **16** 14244
[2] Sato T, Tokunaga K and Tanaka K 2008 *J. Phys. Chem. A* **112** 758
[3] Sato T, Uejima M, Iwahara N, Haruta N, Shizu K and Tanaka K 2013 *J. Phys. Conf. Ser.* **428** 012010
[4] Uejima M, Sato T, Tanaka K and Kaji H 2014 *Chem. Phys.* **430** 47
[5] Kameoka Y, Uebe M, Ito A, Sato T and Tanaka K 2014 *Chem. Phys. Lett.* **615** 44
[6] Uejima M, Sato T, Detani M, Wakamiya A, Suzuki F, Suzuki H, Fukushima T, Tanaka K, Murata Y, Adachi C and Kaji H 2014 *Chem. Phys. Lett.* **602** 80
[7] Uebe M, Ito A, Kameoka Y, Sato T and Tanaka K 2015 *Chem. Phys. Lett.* **633** 190
[8] Endo A, Ogasawara M, Takahashi A, Yokoyama D, Kato Y and Adachi C 2009 *Adv. Mater.* **21** 4802
[9] Uoyama H, Goushi K, Shizu K, Nomura H and Adachi C 2012 *Nature* **492** 234
[10] Kaji H, Suzuki H, Fukushima T, Shizu K, Suzuki K, Kubo S, Komino T, Suzuki F, Wakamiya A, Murata Y, Adachi C 2015 *Nature Commun.* **6** 8476
[11] As a review article, Adachi C 2014 *Jpn. J. Appl. Phys.* **53** 060101
[12] Sato T, Uejima M, Tanaka K, Kaji H and Adachi C 2015 *J. Mater. Chem. C* **3** 870
[13] Sato T 2015 *J. Comput. Chem., Jpn.* **14** 189
[14] Sato T, Hayashi R, Haruta N and Pu Y -J arXiv:1609.06122 [cond-mat.mtrl-sci], 20 Sep 2016.
[15] Yao L, Zhang S, Wang R, Li W, Shen F, Yang B and Ma Y 2014 *Angew. Chem.* **126** 2151
[16] Zhao Y and Truhlar D 2008 *Theor. Chem. Acc.* **120** 215
[17] Frisch M J, Trucks G W, Schlegel H B, Scuseria G E, Robb M A, Cheeseman J R, Scalmani G, Barone V, Mennucci B, Petersson G A, Nakatsuji H, Caricato M, Li X, Hratchian H P, Izmaylov A F, Bloino J, Zheng G, Sonnenberg J L, Hada M, Ehara M, Toyota K, Fukuda R, Hasegawa J, Ishida M, Nakajima T, Honda Y, Kitao O, Nakai H, Vreven T, Montgomery Jr. J A, Peralta J E, Ogliaro F, Bearpark M, Heyd J J, Brothers E, Kudin K N, Staroverov V N, Kobayashi R, Normand J, Raghavachari K, Rendell A, Burant J C, Iyengar S S, Tomasi J, Cossi M, Rega N, Millam J M, Klene M, Knox J E, Cross J B, Bakken V, Adamo C, Jaramillo J, Gomperts R, Stratmann R E, Yazyev O, Austin A J, Cammi R, Pomelli C, Ochterski J W, Martin R L, Morokuma K, Zakrzewski V G, Voth G A, Salvador P, Dannenberg J J, Dapprich S, Daniels A D, Farkas O, Foresman J B, Ortiz J V, Cioslowski J and Fox D J 2009 *Gaussian 09 revision D.01* Gaussian Inc. Wallingford CT
[18] Uejima 2014 PhD Thesis Kyoto University